Evaluation of GaAsSb/AlGaAs strained superlattice photocathodes

Wei Liu, Yiqiao Chen, Aaron Moy, Matthew Poelker, Marcy Stutzman, and Shukui Zhang

Citation: AIP Advances **8**, 075308 (2018); doi: 10.1063/1.5040593
View online: https://doi.org/10.1063/1.5040593
View Table of Contents: http://aip.scitation.org/toc/adv/8/7
Published by the American Institute of Physics

AIP | Conference Proceedings
Get 30% off all print proceedings!
Enter Promotion Code PDF30 at checkout

AIP ADVANCES **8**, 075308 (2018)

Evaluation of GaAsSb/AlGaAs strained superlattice photocathodes

Wei Liu,[1,2,3,a] Yiqiao Chen,[4] Aaron Moy,[4] Matthew Poelker,[3]
Marcy Stutzman,[3] and Shukui Zhang[3]
[1]*Institute of Modern Physics, Chinese Academy of Sciences, 509 Nanchang Rd., Lanzhou 730000, China*
[2]*University of Chinese Academy of Sciences, 19A Yuquan Rd., Beijing 100049, China*
[3]*Thomas Jefferson National Accelerator Facility, 12000 Jefferson Avenue, Newport News, Virginia 23606, USA*
[4]*SVT Associates, Inc. 7620 Executive Dr., Eden Prairie, Minnesota 55344, USA*

(Received 18 May 2018; accepted 26 June 2018; published online 11 July 2018)

GaAs-class strained superlattice (SSL) photocathodes can provide electron beams with electron spin polarization (ESP) exceeding the theoretical maximum 50% of bulk GaAs. In this paper, we describe the evaluation of a SSL structure composed of GaAsSb/AlGaAs and grown on a GaAs substrate. Theoretical analysis and numerical calculations show GaAsSb/AlGaAs SSL structures have the largest heavy-hole and light-hole energy splitting of all existing GaAs-class SSL structures, which should lead to the highest initial ESP. Five GaAsSb/AlGaAs SSL photocathode samples with different constituent species concentrations, number of layer pairs, and layer thicknesses were fabricated and evaluated. The highest ESP was ~77% obtained from a photocathode based on the $GaAsSb_{0.15}/Al_{0.38}GaAs$ (1.55/4.1 nm ×15 layer pairs) SSL structure. © *2018 Author(s). All article content, except where otherwise noted, is licensed under a Creative Commons Attribution (CC BY) license (http://creativecommons.org/licenses/by/4.0/).* https://doi.org/10.1063/1.5040593

I. INTRODUCTION

Spin-polarized electron sources are required for high energy and nuclear physics research, including the study of nuclear structure, the dynamics of strong interactions and electro-weak nuclear physics.[1] Early polarized electron sources relied on bulk GaAs, which can provide high photoelectron yield, or quantum efficiency (QE), but spin polarization cannot exceed 50% because of the degeneracy between heavy-hole (hh) and light-hole (lh) valence energy bands.[2,3] Strained GaAs can provide higher spin polarization because the strain eliminates the degeneracy of the valence band[4] but the strain can only be maintained in thin layers resulting in low QE. To prevent strain relaxation and to increase QE, strained superlattice (SSL) structures consisting of thin quantum well layers and alternating barrier layers were developed.[5] High polarization photocathodes based on AlGaAs/GaAs,[6] InGaAs/GaAs,[7] GaAs/GaAsP,[8] AlInGaAs/GaAsP,[9] InGaAs/AlGaAs,[10] AlInGaAs/AlGaAs[11] SSL structures have been reported in literature. To date, the highest ESP has been obtained from GaAs/GaAsP and AlInGaAs/AlGaAs SSL structures.[11,12]

Besides identifying photocathodes that provide high ESP, many polarized electron-beam science initiatives require high QE and long photogun operating lifetime. It is well known that GaAs photocathodes are very sensitive to ion bombardment, the process whereby residual gas in the high voltage chamber is ionized by the electron beam. The positive ions created by the electron beam are accelerated toward the photocathode that is biased at negative high voltage. The ions can sputter away the chemical layer used to create the necessary negative electron affinity condition, or they are implanted producing interstitial defects or vacancies in the crystal structure which reduce the

[a]Electronic mail: weiliu1006@yahoo.com

 © Author(s) 2018

electron diffusion length.[13] In a previous study,[14,15] a GaAs/GaAsP SSL photocathode was grown atop a distributed Bragg reflector (DBR) structure which served to enhance the absorption of incident laser light, with QE increased by a factor of seven. Although still sensitive to ion bombardment, such a QE enhancement significantly prolongs the operating lifetime of the photocathode, making it easier to sustain beam delivery at a particular beam current for a longer period of time.

In this study, we sought to develop a high-polarization photocathode with high ESP and QE, and also with increased robustness to withstand operation in the electron gun. Using theoretical design principles, strained GaAsSb/AlGaAs SSL structures were developed anticipating higher ESP compared to other structures as a result of larger valence band offset between the quantum well and barrier layers (i.e., the relative alignment of the discontinuous energy bands between layer pairs). For example, the valence band offset is as much as 0.407 eV for the $GaAsSb_{0.15}/Al_{0.38}GaAs$ heterostructure, while it is only 0.155 eV for $GaAs/GaAsP_{0.33}$.[16] Furthermore, antimonides have the smallest effective mass for holes among all the III-V materials including arsenides, phosphides, antimonides and nitrides. The large valence band offset and small hole effective mass will produce large hh-lh energy splitting (ΔE_{hh-lh}), resulting in high initial ESP and a broader high-polarization window (i.e., the range of illumination wavelengths that provide high ESP).

The GaAsSb/AlGaAs SSL can be grown directly on GaAs substrates (with an epitaxially grown GaAs buffer layer) and there will be no strain relaxation in AlGaAs layers because of the near perfect lattice match between AlGaAs and GaAs. Unlike the GaAs/GaAsP SSL which requires a strain relaxed GaAsP layer, no strained material layer will be introduced before growing GaAsSb/AlGaAs SSL structures, resulting in much better material quality with lower defect density which should lead to higher QE. Additionally, GaAsSb/AlGaAs SSL will be more cost-effective than GaAs/GaAsP SSL due to the absence of the thick graded GaAsP buffer. Moreover, GaAsSb, especially highly-strained GaAsSb, has higher electron mobility than GaAs and smaller effective electron mass, which favors faster electron transport, thus reducing the probability of spin relaxation. Here, five GaAsSb/AlGaAs SSL photocathode samples with different alloy compositions, number of layer pairs, and layer thickness were manufactured and evaluated using a retarding-field Mott polarimeter.

II. THEORY

A schematic of the $GaAsSb_x/Al_yGaAs$ SSL photocathode evaluated in this study is shown in Table I. The SSL layers were grown between a spacer layer of Al_yGaAs and a heavily-doped GaAs cap layer. The heavily doped cap layer enhances the negative electron affinity (NEA) surface condition to improve the electron escape probability and minimize the phenomenon known as surface charge limit that restricts the maximum charge that can be extracted from a photocathode.[17,18] The SSL layers have low doping in order to increase electron mobility and reduce depolarization due to scattering. The $GaAsSb_x$ layers are quantum-well layers and the Al_yGaAs layers are barrier layers. This structure provides a compressive biaxial strain induced in the $GaAsSb_x$ layers to alter the energy band structure of the photocathode, to eliminate the degeneracy of the valence band.

A $\boldsymbol{k}\cdot\boldsymbol{p}$ model based on the Luttinger-Kohn Hamiltonian that takes into account strain effects (also called Pikus-Bir Hamiltonian[19]) was used to estimate the band structure of the SSL photocathodes.[20] This Hamiltonian can be described by a 4×4 matrix, which takes into account the heavy-hole and light-hole bands.[21] Using a unitary transformation, the 4×4 Hamiltonian can be block diagonalized into two 2×2 Hamiltonians.[22] For a quantum-well without strain, where the structure is symmetric,

TABLE I. The schematic of the $GaAsSb_x/Al_yGaAs$ SSL photocathode.

Layer	Thickness (nm)	Doping density (cm^{-3})
GaAs	5	5×10^{19}
$GaAsSb_x/Al_yGaAs$	~100	5×10^{17}
Al_yGaAs	250	5×10^{18}
GaAs buffer	200	7×10^{18}
	GaAs substrate ($p > 5 \times 10^{17} cm^{-3}$)	

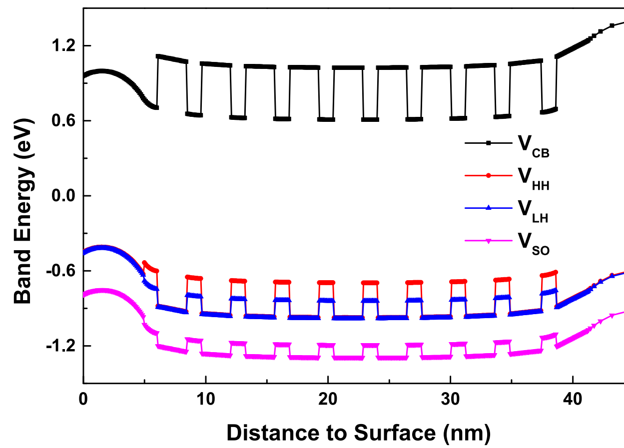

FIG. 1. The calculated flat-band structure of a $GaAsSb_{0.147}/Al_{0.38}GaAs$ (1.2/2.4 nm ×10 layer pairs) SSL photocathode, including the band energy of conduction band (CB), heavy-hole band (HH), light-hole band (LH) and split-off band (SO). The SSL bandgap (E_g) is 1.602 eV, and the hh-lh energy splitting (ΔE_{hh-lh}) is 131.7 meV.

the solutions for both Hamiltonians are degenerate, thus only one 2 × 2 matrix must be solved to find the band energy. For a quantum-well with strain, where the structure does not have inversion symmetry, the upper and lower Hamiltonians are decoupled, and thus both the upper and lower Hamiltonians are required and the 2 × 2 matrix for each block of the Hamiltonian must be solved.

For a $GaAsSb_{0.147}/Al_{0.38}GaAs$ SSL structure, the estimated flat-band structure is shown in Figure 1. For this figure, the spacer layer was $Al_{0.38}GaAs$. The compressive strain within the quantum well layers shifts the heavy-hole band above the light-hole band providing an energy splitting of 131.7 meV. At the photocathode surface, and at the spacer layer, bands are bent at the interface between layers where dopant concentrations are different. The bandgap of the $GaAsSb_{0.147}/Al_{0.38}GaAs$ SSL at $\boldsymbol{k} = 0$ (Γ point) was 1.602 eV, corresponding to a maximum ESP at a laser illumination wavelength of 774 nm, which is easily accessible using frequency-doubled telecommunications diode lasers like those used at Jefferson Lab for nuclear physics research.[23]

As mentioned above, the GaAsSb/AlGaAs SSL structures can produce large hh-lh energy splitting because of the large valence band offset and small hole effective mass. The hh-lh energy splitting for different existing GaAs-class SSL structures[5–11,24,25] are shown in Table II. From this table, one can see that the GaAsSb/AlGaAs SSL structures exhibit the largest hh-lh energy splitting, which should lead to highest initial spin polarization and broadest high-polarization wavelength window.

The bandgap and hh-lh energy splitting of the $GaAsSb_x/Al_yGaAs$ SSL photocathode can be tuned to specific values by adjusting the fraction (x) of Sb in $GaAsSb_x$ layers and the fraction (y) of Al in the Al_yGaAs layers, as shown in Figure 2. The red lines show the change in the bandgap and hh-lh energy splitting as a function of Sb fraction for a fixed Al fraction (y = 0.38). The blue lines show the change in bandgap and energy splitting as a function of Al fraction for a fixed Sb

TABLE II. The hh-lh energy splitting (ΔE_{hh-lh}) for different SSL structures.

SSL structure	ΔE_{hh-lh} (meV)
GaAsSb/AlGaAs	101-155
AlGaAs/GaAs[5,6]	20-44
GaAs/GaAsP[8,10,24]	35-89
$In_{0.15}GaAs/GaAs$[7]	70
InGaAs/AlGaAs[10]	80-104
AlInGaAs/GaAs[25]	59-79
AlInGaAs/GaAsP[9]	27-44
AlInGaAs/AlGaAs[11]	61-87

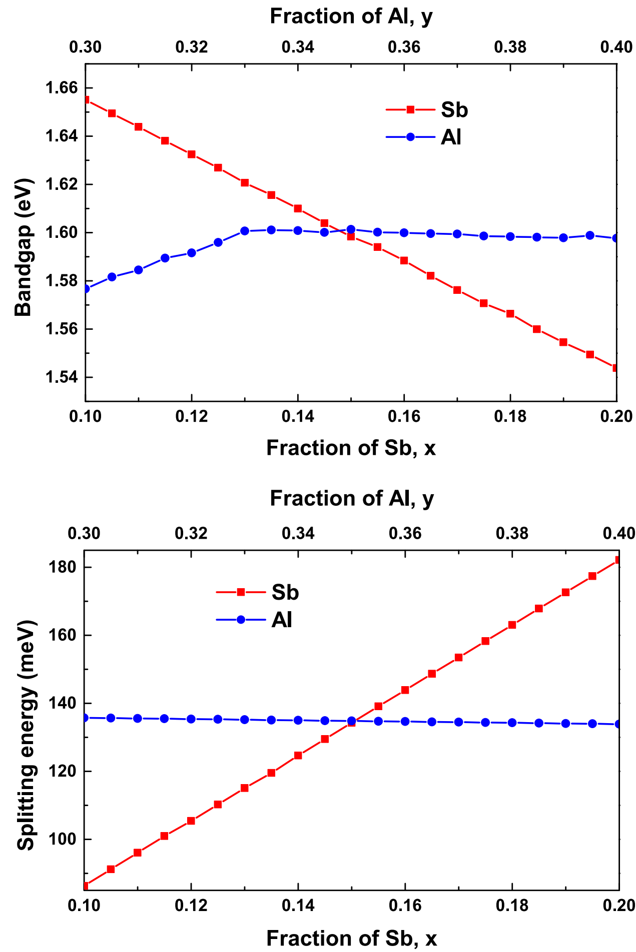

FIG. 2. (top) The bandgap (E_g) and (bottom) hh-lh energy splitting (ΔE_{hh-lh}) of GaAsSb$_x$/Al$_y$GaAs (1.2/2.4 nm ×10 layer pairs) SSL as function of Sb fraction (x) in the GaAsSb$_x$ layers (red line, y=0.38) and the Al fraction in Al$_y$GaAs layers (blue line, x=0.15).

fraction (x = 0.15). The fraction of Sb in GaAsSb$_x$ layers has a strong effect on the bandgap and hh-lh energy splitting. Increasing the fraction of Sb reduces the bandgap and significantly increases the hh-lh energy splitting. However, the Al fraction has only a weak effect on the bandgap and energy splitting. For an Al fraction greater than 0.33, the bandgap energy is nearly constant. The hh-lh energy splitting has only a very weak dependence on Al fraction.

III. EXPERIMENT AND RESULTS

All of the photocathodes were grown in a solid-source molecular beam epitaxy (SSMBE) system equipped with antimony (Sb) and arsenic (As) crackers. First, a 200 nm Be-doped (7×10^{18} cm^{-3}) GaAs buffer layer was deposited onto a p-type GaAs substrate (doping density > 5×10^{17} cm^{-3}). Then a 250 nm Be-doped (5×10^{18} cm^{-3}) Al$_y$GaAs layer was grown upon the buffer to produce a strain-relaxed layer compatible with the p-type (5×10^{17} cm^{-3}) SSL. The GaAsSb$_x$/Al$_y$GaAs SSL was then fabricated, with up to 30 layer pairs. Next, a 5 nm highly p-doped (5×10^{19} cm^{-3}) GaAs layer was grown, to improve the electron escape probability and reduce the likelihood of surface charge limit. Finally, the surface of the photocathode was covered with an arsenic cap layer, to preserve photocathode cleanliness during handling. Five photocathode samples were manufactured with varying alloy compositions, number of layer pairs, and layer thicknesses of the SSL structure. The parameters of each sample are shown in Table III.

TABLE III. The maximum ESP measured at any wavelength λ with corresponding QE for five photocathode samples, together with the SSL structure parameters and calculated values of bandgap E_g and hh-lh energy splitting ΔE_{hh-lh}.

Sample	Parameters of SSL	E_g (eV)	ΔE_{hh-lh} (meV)	Max ESP at λ	QE(%)
1	$GaAsSb_{0.173}/Al_{0.4}GaAs$ (1.2/4 nm ×20 layer pairs)	1.572	155.3	73.1% at 790 nm	0.041
2	$GaAsSb_{0.165}/Al_{0.4}GaAs$ (1.2/4 nm ×20 layer pairs)	1.581	148.6	73.9% at 780 nm	0.27
3	$GaAsSb_{0.15}/Al_{0.38}GaAs$ (1.55/4.1 nm ×15 layer pairs)	1.599	134.3	76.7% at 795 nm	0.33
4	$GaAsSb_{0.147}/Al_{0.38}GaAs$ (1.2/2.4 nm ×30 layer pairs)	1.602	131.7	74.8% at 780 nm	0.62
5	$GaAsSb_{0.115}/Al_{0.38}GaAs$ (1.2/2.4 nm ×30 layer pairs)	1.638	101	75.6% at 750 nm	0.46

Photocathode samples were evaluated using an ultra-high vacuum system that encompasses an electron source chamber and low-voltage retarding-field Mott polarimeter.[26] A schematic of the experimental apparatus is shown in Figure 3. Photocathodes were attached to a sample holder and introduced into the vacuum apparatus using a long bellows load-lock system. Before opening a valve to the polarimeter, the sample and holder were baked under vacuum at 250°C for 12 hours and then allowed to cool to room temperature, to achieve a typical vacuum pressure ~ 10^{-11} Torr. Following this, photocathode samples could then be moved into place within the polarimeter, where the photocathode was heated to 480°C to remove the arsenic cap prior to activation at room temperature with cesium and NF_3 to create the NEA condition using the standard yo-yo activation procedure.[27] The cathode was illuminated using a broadly tunable super-continuum laser (NKT Photonics, SuperK) that could provide milli-Watts of output power over the wavelength range 400 to 800 nm. Spin polarized photoemission requires illumination with circularly polarized light, which was obtained using a simple quarter-wave retardation plate following a linear polarizer. The orientation of the spin direction could be flipped 180° using an insertable half-wave retardation plate.

To deliver an electron beam to the Mott scattering target, the photocathode sample (element a in Figure 3) was biased at -268 V using a battery bias box, and the photocurrent was monitored with a picoammeter. The longitudinally polarized electron beam was bent 90° by an electrostatic bend (elements b and c), forming a transversely polarized electron beam required by Mott scattering

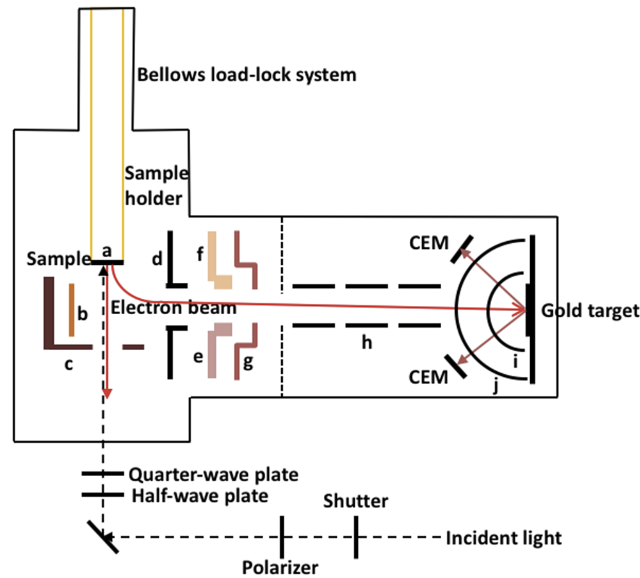

FIG. 3. Schematic of the experimental apparatus, with electron source chamber, transport lenses (d-g) and low-voltage retarding field Mott Polarimeter. The spin direction of the photoemitted electrons is parallel to the direction of motion at the photocathode. A deflector element (b, c) directs the beam to the Mott target and also rotates the spin direction 90°, which is a requirement for Mott scattering polarimetry. The voltage applied to elements (b-g) can be adjusted to optimize the transmission of electrons to the target.

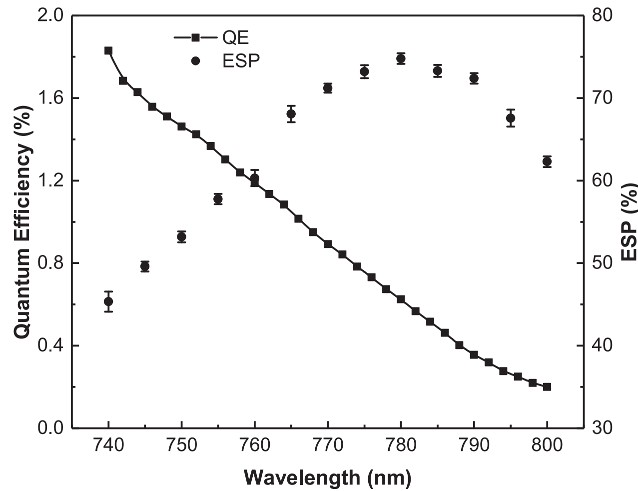

FIG. 4. The Quantum Efficiency and ESP for sample 4: $GaAsSb_{0.147}/Al_{0.38}GaAs$ (1.2/2.4 nm ×30 layer pairs) as a function of wavelength. Error bars are statistical.

polarimetry. The transversely polarized electron beam was focused and steered to the thick gold target within the Mott polarimeter using a split lens (elements f and e), two cylindrical lenses (elements d and g) and three tube lenses. Only a portion of the electron beam reaches the Mott scattering target. Adjusting the voltage applied to the transport lenses helped to obtain the best transmission necessary for efficient data collection and analysis. The Mott polarimeter accelerates the electron beam to 20 kV between the inner and outer hemispheres (elements i and j), scatters the electrons at 20 kV, then decelerates the scattered electrons back to the transport energy of 268 eV before the asymmetry between right and left scattering is detected in two channel electron multipliers.

The measured values of QE and ESP are shown in Table III for the five GaAsSb/AlGaAs SSL photocathode samples, together with the SSL structure parameters and calculated values of bandgap and hh-lh energy splitting. All the samples have calculated hh-lh energy splitting greater than 100 meV and bandgap near 1.6 eV. For three of the five samples, the maximum ESP was obtained at laser wavelengths significantly different from their design value of 780 nm. Sample No. 4 ($GaAsSb_{0.147}/Al_{0.38}GaAs$ (1.2/2.4 nm ×30 layer pairs) SSL photocathode) provided the best results, exhibiting the highest ESP of 74.8% and QE of 0.62% at ~780 nm. The QE and ESP for this sample are shown in Figure 4 as a function of illumination wavelength. The QE spectrum does not indicate the characteristic step variation typically observed for GaAs/GaAsP SSL photocathodes[8] associated with distinct transitions to the conduction band from the heavy hole and light hole bands. The reason of this will be discussed in the next section. All of the photocathode samples provided similar maximum ESP values but with lower QE.

IV. DISCUSSION

As illustrated in Section II, alloy composition and layer thickness of the quantum well and barrier layers in the SSL structure determine the energy band structure of the photocathode, which in turn determines the QE and ESP obtained from the photocathode. The Sb fraction in $GaAsSb_x$ quantum well layers has a strong effect on the bandgap which determines the wavelength (or photon energy) corresponding to the maximum ESP of photocathode, and the hh-lh energy splitting that influences value of maximum ESP. In contrast, the Al fraction in Al_yGaAs barrier layers has only a slight effect on the bandgap and hh-lh energy splitting.

Theoretical analysis and numerical calculations were presented that predict the GaAsSb/AlGaAs SSL structure to have the largest hh-lh energy splitting of all existing GaAs-class SSL structures and therefore suggests the GaAsSb/AlGaAs SSL photocathode will provide very high ESP. For example, the hh-lh energy splitting can be as high as 131.7 meV for the $GaAsSb_{0.147}/Al_{0.38}GaAs$ SSL structure,

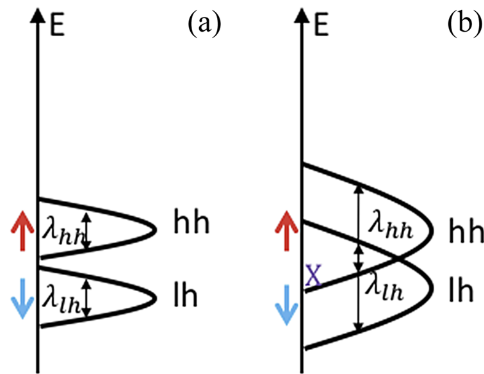

FIG. 5. The heavy-hole and light-hole band distribution of SSL structures. (a) Ideal condition: the SSL strain is large enough and the bandwidths (λ) of heavy-hole and light-hole are small, so that the heavy-hole and light-hole are completely separated; (b) Non-ideal condition: the SSL strain is not large enough and the band widths of heavy-hole and light-hole are large, so that heavy-hole and light-hole energy bands are mixed.

compared to 89 meV of widely used GaAs/GaAsP SSL photocathode[8] which provides ESP ~86% and QE ~1%. But despite these optimistic predictions, the GaAsSb/AlGaAs SSL photocathode samples described here provided only ~75% ESP and QE $< 1\%$. There are some likely explanations for these results.

The bandwidths of the heavy-hole and light-hole bands (λ_{hh} and λ_{lh}) were not considered in the band structure calculation. When the heavy-hole and light-hole bands of the SSL structure are completely separated, as shown in Figure 5(a), the initial ESP would be 100%. However, lower ESP will be observed if the heavy-hole and light-hole bands are not completely separated, as shown in Figure 5(b). The strained quantum-well layer for a GaAs/GaAsP SSL is GaAs, whereas the strained quantum-well layer for a GaAsSb/AlGaAs SSL is GaAsSb. We speculate that the bandwidths of the heavy-hole and light-hole bands of the GaAsSb/AlGaAs SSL were larger than expected and more like that shown in Figure 5(b). So, although the hh-lh energy splitting of the GaAsSb/AlGaAs SSL was larger than that of the GaAs/GaAsP SSL, there was incomplete separation of the heavy-hole and light-hole bands, resulting in relatively low ESP. This can also explain why the QE spectrum of the GaAsSb/AlGaAs SSL photocathodes did not exhibit the characteristic step variation corresponding to the distinct excitation transitions from heavy-hole and light-hole bands to the conduction band.

Another possible explanation for low ESP and QE relates to sample fabrication. Our fabrication technology for strained GaAsSb/AlGaAs SSL structures is not very mature, causing insufficient control of some parameters, such as the alloy composition and layer thickness. The band structure of a SSL structure is very sensitive to these parameters, especially the fraction of Sb in the GaAsSb layers.

Furthermore, the model could be enhanced to include potentially significant effects that might explain lower than expected ESP and QE, such as the impact of hh-lh mixing. Similarly, the role of spin-exchange interaction on the hole states should be considered for thin superlattice layers, which can be obtained by multi-particle calculations.[28] The influence of spin relaxation could be an important consideration, especially for highly doped semiconductor layers that might even become degenerate in the conduction band.[29] Finally, the effect of the piezoelectric effect applied to the highly doped superlattice layers should be considered, which could influence the electron and hole charge distributions.[30]

Future work includes efforts to optimize the simulation and calculation methods to obtain more detailed and accurate band structure predictions, so that a more accurate model exists to assist fabrication of the ideal photocathode. Fabrication techniques should be improved to achieve better QE and ESP. And finally, the GaAsSb/AlGaAs SSL photocathode samples should be evaluated inside a high voltage photogun, to experimentally evaluate the possible decrease in the sensitivity to ion bombardment.

ACKNOWLEDGMENTS

Authored by Jefferson Science Associates, LLC under U.S. DOE Contract No. DE-AC05-06OR23177. The U.S. Government retains a non-exclusive, paid-up, irrevocable, world-wide license to publish or reproduce this manuscript for U.S. Government purposes. SVT Associates was funded by the U.S. DOEs Office of Nuclear Physics SBIR program DE-SC0009516.

[1] H. Montgomery, J. Phys. Conf. Ser. **299**, 11001 (2011).
[2] D. T. Pierce and F. Meier, Phys. Rev. B **13**, 5484 (1976).
[3] W. Liu, M. Poelker, X. Peng, S. Zhang, and M. Stutzman, J. Appl. Phys. **122**, 035703 (2017).
[4] T. Maruyama, E. L. Garwin, R. Prepost, G. H. Zapalac, J. S. Smith, and J. D. Walker, Phys. Rev. Lett. **66**, 2376 (1991).
[5] T. Omori, Y. Kurihara, T. Nakanishi, H. Aoyagi, T. Baba, T. Furuya, K. Itoga, M. Mizuta, S. Nakamura, Y. Takeuchi, M. Tsubata, and M. Yoshika, Physcial Rev. Lett. **67**, 3294 (1991).
[6] S. F. Alvarado, F. Ciccacci, and M. Campagna, Appl. Phys. Lett. **39**, 615 (1981).
[7] T. Omori, Y. Kurihara, Y. Takeuchi, M. Yoshioka, T. Nakanishi, S. Okumi, M. Tsubata, M. Tawada, K. Togawa, Y. Tanimoto, C. Takahashi, T. Baba, and M. Mizuta, Jpn. J. Appl. Phys. **33**, 5676 (1994).
[8] T. Maruyama, D. A. Luh, A. Brachmann, J. E. Clendenin, E. L. Garwin, S. Harvey, J. Jiang, R. E. Kirby, C. Y. Prescott, R. Prepost, and A. M. Moy, Appl. Phys. Lett. **85**, 2640 (2004).
[9] A. V. Subashiev, L. G. Gerchikov, Y. A. Mamaev, Y. P. Yashin, J. S. Roberts, D.-A. Luh, T. Maruyama, and J. E. Clendenin, Appl. Phys. Lett. **86**, 171911 (2005).
[10] T. Nishitani, T. Nakanishi, M. Yamamoto, S. Okumi, F. Furuta, M. Miyamoto, M. Kuwahara, N. Yamamoto, K. Naniwa, O. Watanabe, Y. Takeda, H. Kobayakawa, Y. Takashima, H. Horinaka, T. Matsuyama, K. Togawa, T. Saka, M. Tawada, T. Omori, Y. Kurihara, M. Yoshioka, K. Kato, and T. Baba, J. Appl. Phys. **97**, 94907 (2005).
[11] Y. A. Mamaev, L. G. Gerchikov, Y. P. Yashin, D. A. Vasiliev, V. V. Kuzmichev, V. M. Ustinov, A. E. Zhukov, V. S. Mikhrin, and A. P. Vasiliev, Appl. Phys. Lett. **93**, 81114 (2008).
[12] X. Jin, B. Ozdol, M. Yamamoto, A. Mano, N. Yamamoto, and Y. Takeda, Appl. Phys. Lett. **105**, 203509 (2014).
[13] W. Liu, S. Zhang, M. Stutzman, and M. Poelker, Phys. Rev. Accel. Beams **19**, 103402 (2016).
[14] S. Zhang, M. L. Stutzman, M. Poelker, Y. Chen, and A. Moy, Proc. IPAC2015 TUPMA038, 1923 (2015).
[15] W. Liu, Y. Chen, W. Lu, A. Moy, M. Poelker, M. Stutzman, and S. Zhang, Appl. Phys. Lett. **109**, 252104 (2016).
[16] I. Vurgaftman, J. R. Meyer, and L. R. Ram-Mohan, J. Appl. Phys. **89**, 5815 (2001).
[17] M. Woods, J. Clendenin, J. Frisch, A. Kulikov, P. Saez, D. Schultz, J. Turner, K. Witte, and M. Zolotorev, J. Appl. Phys. **73**, 8531 (1993).
[18] A. Herrera-Gómez, G. Verqara, and W. E. Spicer, J. Appl. Phys. **79**, 7318 (1996).
[19] G. E. Pikus and G. L. Bir, Sov. Phys. Solid State **1**, 136 (1959).
[20] S. L. Chuang, Phys. Rev. B **43**, 9649 (1991).
[21] L. C. Andreani, A. Pasquarello, and F. Bassani, Phys. Rev. B **36**, 5887 (1987).
[22] S. L. Chuang, Phys. Rev. B **40**, 10379 (1989).
[23] C. K. Sinclair, P. A. Adderley, B. M. Dunham, J. C. Hansknecht, P. Hartmann, M. Poelker, J. S. Price, P. M. Rutt, W. J. Schneider, and M. Steigerwald, Phys. Rev. Spec. Top. - Accel. Beams **10**, 1 (2007).
[24] T. Maruyama, E. L. Garwin, R. Prepost, and G. H. Zapalac, Physcial Rev. B **46**, 4261 (1992).
[25] L. G. Gerchikov, Y. A. Mamaev, A. V. Subashiev, Y. P. Yashin, D. A. Vasil'ev, V. V. Kuz'michev, A. E. Zhukov, E. S. Semenova, A. P. Vasil'ev, and V. M. Ustinov, Semiconductors **40**, 1326 (2006).
[26] J. L. McCarter, M. L. Stutzman, K. W. Trantham, T. G. Anderson, A. M. Cook, and T. J. Gay, Nucl. Instruments Methods Phys. Res. Sect. A **618**, 30 (2010).
[27] F. Ciccacci and G. Chiaia, J. Vac. Sci. Technol. A **9**, 2991 (1991).
[28] P. Klenovský, P. Steindl, and D. Geffroy, Sci. Rep. **7**, 45568 (2017).
[29] J. S. Blakemore, J. Appl. Phys. **53**, R123 (1982).
[30] J. Aberl, P. Klenovský, J. S. Wildmann, J. Martín-Sánchez, T. Fromherz, E. Zallo, J. Humlíček, A. Rastelli, and R. Trotta, Phys. Rev. B **96**, 045414 (2017).